Performance analysis of dual-hop underwater visible light communication system with receiver diversity

Rachna Sharma* and **Yogesh N. Trivedi**
Nirma University, Institute of Technology, Ahmedabad, Gujarat, India

Abstract. Visible light communication (VLC) has the ability to provide a high data rate up to Mbps in underwater environments for real-time communication systems. In underwater VLC (UWVLC), two major impairments are the turbulence-induced fading due to variation of salt and temperature of seawater and incremental path loss with distance due to absorption and scattering. We consider these two impairments and derive the closed form expressions for average symbol error probability (ASEP), asymptotic relative diversity order, and ergodic capacity for UWVLC dual-hop cooperative communication system. We consider multiple receiver branches with selection combining to combat the effect of fading. The impact of temperature on the fading parameters and system performance is highlighted. We conduct a comparative analysis of ASEP for four-pulse amplitude modulation and four-square quadrature amplitude modulation schemes and draw useful insights. We prove the accuracy of the derived analytical expression using Monte Carlo simulations. © *2021 Society of Photo-Optical Instrumentation Engineers (SPIE)* [DOI: 10.1117/1.OE.60.3.035111]

Keywords: underwater visible light communication; underwater turbulence; average symbol error rate probability; relative diversity order; ergodic capacity.

Paper 20201466 received Dec. 16, 2020; accepted for publication Mar. 10, 2021; published online Mar. 30, 2021.

1 Introduction

Recently, maritime activities, such as environmental monitoring, port security, oceanographic data collection, and tactical surveillance, have been expanding their scope. As a result, there is a growing demand for high-speed underwater wireless communication systems.[1,2] Acoustic underwater communication (UWC) has received attention in the last few decades because it can support a transmission range up to tens of kilometers. However, acoustic waves fail to support a high data rate.[3] Further, as the speed of the acoustic signal in water is quite low, there is a challenge of latency that needs to be dealt with. In addition, the acoustic band has a very small bandwidth, which makes it increasingly difficult to have high data rates in hundreds of Mbps.[4] Due to these limitations of acoustic communication, underwater visible light communication (UWVLC) is emerging as an envisioned alternative to acoustics communication. Optical wireless communication (OWC) has the capacity to dominate the market of underwater wireless communication due to its low latency. It has lately been applied to many underwater applications such as imaging and real-time video transmission, and the results have surely been encouraging.[1,2] The OWC supports information transmission in the wavelength range of 100 nm to 1 mm utilizing light sources such as light-emitting diodes and laser diodes.[5] The experimental results have shown that attenuation is minimum in the wavelength range of 520 to 560 nm for applications involving coastal water.[6] Looking at the current trends, the commercial market of underwater optical modems, which are currently available up to data rates of 500 Mbps, can be expected to grow at a fast rate.[5,7]

Underwater, the refractive index of the water varies with depth. This leads to abrupt changes in the average power received, thereby creating optical turbulence.[8,9] Further, the density of the water increases with depth in underwater. The density of seawater is inversely proportional to temperature and directly proportional to pressure and salinity. However, the effect of the pressure

*Address all correspondence to Rachna Sharma, rachna.sharma@nirmauni.ac.in

is usually neglected.[8,10] Therefore, variation in the refractive index, by and large, depends upon the change in temperature and salinity. Exhaustive research has been conducted to show the impact of attenuation and scattering on optical carriers for UWC.[6,11–13] The impact of eddy diffusivity on turbulence-induced fading has been explored and incorporated in different channel models for the varying depth of water.[14–17] Mohammed et al. modeled the irradiance fluctuations due to the weak turbulence of water using lognormal distribution.[15,18] The effect of strong turbulence in UWVLC has been investigated, in which a vertical channel was modeled with the help of cascaded independent non-identically distributed gamma–gamma probability density function (PDF).[17,18]

Diversity plays a major role to improve the performance in UWC.[4,19–21] Yilmaz et al.[4] analyzed performance for vertical UWVLC link for various transceivers. Moreover, the transmitter diversity has been explored in Refs. 22 and 23 and the system performance was analyzed considering weak turbulence. Elamassie et al.[11] presented a closed-form expression for path loss assuming serial equidistant UWVLC system using amplify-and-forward (AF) and decode-and-forward (DF) relay and derived the maximum distance for a targeted bit error rate (BER), however, the effect of turbulence has not been considered.

The on-off keying (OOK) and pulse amplitude modulation (PAM) have been widely used as preferred modulation techniques in UWVLC. However, the poor spectral efficiency exhibited by OOK and PAM has made quadrature amplitude modulation (QAM) a more often used technique due to its ability of being able to possess high spectral efficiency.[24,25]

This paper considers a dual-hop DF relayed UWVLC system, where one laser source is available at the transmitter and N photodetectors at the destination. The relay is equipped with a single-laser source and a photodetector and placed in the middle of the source and destination. The main contribution of this paper is as follows.

- For the considered system, we have derived the closed-form analytical expressions of average symbol error probability (ASEP) and ergodic capacity.
- We have derived the analytical expression of relative diversity order (RDO) for lognormally distributed channel incorporating DF relaying and selection combining (SC) at the receiver. As an important observation, it is demonstrated that in a cooperative relaying system, with receiver diversity used only at the relay to destination link, the diversity order does not improve. However, in such a system, SNR gain is achieved, which increases with the number of receiver branches at the destination node.
- Further, we derive the analytical expression of asymptotic relative diversity order (ARDO) and ergodic capacity and study the effect of temperature on these performance metrics.
- We have demonstrated the effect of variation in the temperature of seawater on the performance for PAM and RQAM schemes. We have also studied the effect of employing multiple photodetectors at the destination node and highlighted the SNR gain achieved.
- Furthermore, we have presented our results using simulations and compared them with their analytical counterparts. A close matching between them validated our analytical expressions of ASEP and ergodic channel capacity.

The remainder of this paper is organized as follows. In Sec. 2, we describe the dual-hop underwater channel and system with the parameters of the scintillation index. In Sec. 3, we present the performance analysis in terms of ARDO, ASEP for PAM and SQAM schemes, and also derive analytical expression for ergodic capacity. Section 4 shows the derived results with Monte Carlo simulations. The conclusions are finally presented in Sec. 5.

2 System and Channel Model

We consider an line-of-sight dual-hop UWVLC cooperative communication system with one laser source at the transmitter node and N photodetectors at the destination node $\mathcal{D}$. The considered system is shown in Fig. 1, where $\mathcal{S}$ is the source node that transmits information to the $\mathcal{D}$ with the assistance of a relay node $\mathcal{R}$, which has a single pair of transmitter and receiver. The distances between source to relay and relay to destination are denoted by L_{SR} and L_{RD}, respectively. The cooperation of a relay assisted system works on half-duplex mode considering the

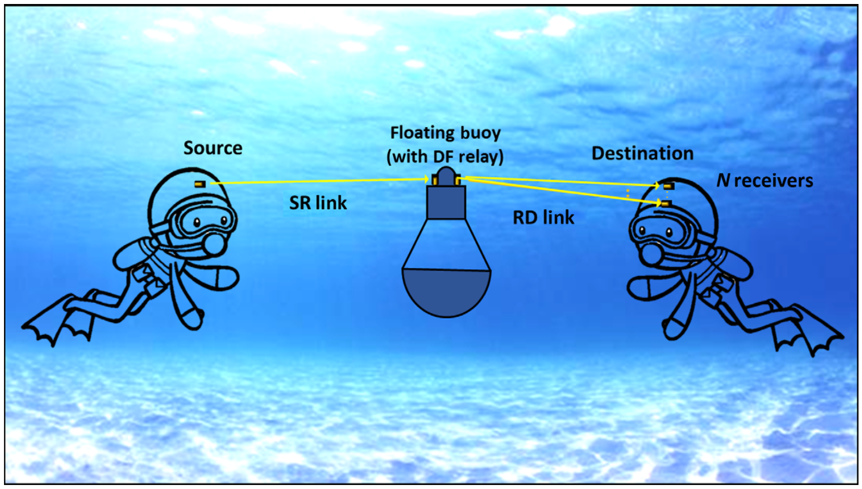

Fig. 1 UWVLC system model.

channel state information (CSI) available at R and D. The $N-\mathcal{R}-\mathcal{D}$ links are considered as independent, and the separation between the photodetectors is kept very small in the orders of centimeters as compared to the transmission range L. The total allocated power $\mathcal{P}$ is divided between $\mathcal{S}$ and $\mathcal{R}$ nodes. Let $\mathcal{P}_S$ and $\mathcal{P}_R$ be the power assigned to $\mathcal{S}$ and $\mathcal{R}$, respectively. The total aperture area (A_r) at the receiver gets divided into N parts, with each part connected to a photodetector.[4,26] Let x be independent and identically distributed (IID) transmitted information symbol with average energy normalized to 1, $\mathbb{E}[|x|^2]=1$. The communication over relayed link takes place in two phases. In the first phase, $\mathcal{S}$ sends the signal to $\mathcal{R}$, and in the second phase, $\mathcal{R}$ sends the signal to the $\mathcal{D}$.

The relay $\mathcal{R}$ receive the signal y_R in the first phase, which can be expressed as[22]

$$y_R = \eta_\circ \mathcal{P}_S I_{SR} h_{SR} x + w_R, \tag{1}$$

where $\eta_\circ$ is the electrical to optical conversion efficiency. The I_{SR} and h_{SR} represent the turbulence induced fading coefficient and attenuation coefficient, respectively. The I_{SR} follows the log-normal distribution under the weak turbulence condition with PDF:[15,18]

$$f_{I_{SR}}(I_{SR}) = \frac{1}{\sqrt{2\pi}\sigma_{I_{SR}} I_{SR}} \exp\left(\frac{-(\ln(I_{SR}) - \mu_{I_{SR}})^2}{2\sigma^2_{I_{SR}}}\right), \tag{2}$$

where $I_{SR} \sim \mathbb{LN}(\mu_{I_{SR}}, \sigma_{I_{SR}})$ and $\ln(\cdot)$ represents the natural logarithm. The mean value of I_{SR} is normalized to 1 by setting $\mu_{I_{SR}} = -0.5\sigma^2_{I_{SR}}$. The w_R is the additive white Gaussian noise (AWGN) with mean 0 the variance $\sigma^2_{w_R}$.[27] The relay $\mathcal{R}$ operates in DF mode. It detects and again modulates the received signal with power $\mathcal{P}_{\mathcal{R}}$ and then sends the signal to the $\mathcal{D}$. The destination $\mathcal{D}$ is equipped with N photodetectors and employs SC. In the SC, we select the photodetector with the highest SNR for detection.

The received signal at the n'th detector is expressed as

$$y_D^{(n)} = \eta_\circ \mathcal{P}_R h_{RD} I_{RD}^{(n)} \hat{x} + w_D^{(n)}, \tag{3}$$

where $1 \le n \le N$.

The detected signal at the relay $\mathcal{R}$ is represented by $\hat{x}$. The h_{RD} is the path loss of $\mathcal{R}-\mathcal{D}$ link, which is normalized to $\mathcal{S}-\mathcal{D}$ link. The $w_D^{(n)}$ represents AWGN with mean value 0 and variance $\sigma^2_{w_D}$.[28] The $I_{RD}^{(n)}$ is the turbulence fading corresponding to the n'th link between $\mathcal{R}$ and $\mathcal{D}$, which follows log-normal distribution, $I_{RD}^{(n)} \sim \mathbb{LN}(\mu_{RD}, \sigma^2_{RD})$, for $n = 1,2,\ldots,N$. $\mathbb{LN}[\cdot]$ represents the log-normal distribution. The path loss depends upon the attenuation, scattering, and geometrical losses. The path loss for a semicollimated laser source with a Gaussian beamshape is defined as[11]

$$h_j \approx \left(\frac{D_R}{Q_F}\right)^2 L_j^{-2} \exp\left(-c\left(\frac{D_R}{Q_F}\right)^{\rho} L_j^{1-\rho}\right), \tag{4}$$

where $j \in \{\mathcal{SR}, \mathcal{RD}\}$, D_R, Q_F, ρ, and c denote receiver aperture diameter, beam divergence angle, correction coefficient, and extinction coefficient, respectively. The L represents the distance in meters. The UWVLC undergoes the irradiance fluctuations due to the variation of temperature and salt of the water, which follows the log-normal distribution under the weak turbulence.[15] The turbulence variance can be represented in terms of scintillation index σ_j^2 as $\sigma_j^2 = \ln(\sigma_{I_j}^2 + 1)$. In the weak turbulence regime, for Gaussian-beam waves propagating through non-Kolmogorov turbulent atmosphere, the receiver-aperture-averaged scintillation index $\sigma_{I_j}^2$ can be expressed as[14,29]

$$\sigma_{I_j}^2 = 8\pi^2 k_0^2 L_j \int_0^1 \int_0^\infty \kappa \Phi_n(\kappa) \exp\left(-\frac{\Lambda L_j \kappa^2 \mathcal{E}^2}{k_0} - \frac{D_R^2 \kappa^2 \mathcal{E}^2}{16}\right) \times \left\{1 - \cos\left[\frac{L\kappa^2}{k_0} \mathcal{E}(1 - (1 - \Theta)\mathcal{E})\right]\right\} \mathrm{d}\kappa\, \mathrm{d}\mathcal{E}, \tag{5}$$

where $\Phi_n(\kappa)$ is the spatial power spectrum model of turbulent fluctuations of the sea-water refraction given by

$$\Phi_n(\kappa) = (4\pi\kappa^2)^{-1} \times C_0\left(\frac{\alpha^2 \chi_T}{\omega^2}\right) \epsilon^{-1/3} \kappa^{-5/3} [1 + C_1(\kappa\eta)^{2/3}] \times [\omega^2 \exp(-C_0 C_1^{-2} P_T^{-1} \delta) + d_r \exp(-C_0 C_1^{-2} P_S^{-1} \delta) - \omega(d_r + 1) \times \exp(-0.5 C_0 C_1^{-2} P_{TS}^{-1} \delta)]. \tag{6}$$

The eddy diffusivity ratio d_r, δ, η, and ω are defined as[14]

$$d_r = \begin{cases} |\omega| / \left(|\omega| - \sqrt{|\omega|(|\omega| - 1)}\right), & |\omega| \geq 1 \\ 1.85|\omega| - 0.85, & 0.5 \leq |\omega| \leq 1 \\ 1.5|\omega|, & |\omega| < 0.5, \end{cases} \qquad \delta = 1.5 C_1^2 (\mathcal{E}\eta)^{(4/3)} + C_1^3 (\mathcal{E}\eta)^2, \tag{7}$$

$$\eta = (v^2/\epsilon)^{1/4}, \tag{8}$$

$$\omega = \alpha\left(\frac{dT}{dZ}\right) / \beta\left(\frac{dS}{dZ}\right). \tag{9}$$

In Eq. (6), P_T is the Prandtl number of temperature, which is a unitless quantity. It is the ratio of kinematic viscosity to molecular thermal diffusivity, defined as $P_T = v/D_T$, where D_T is defined as $D_T = \sigma_T/(\rho \times C_P)$ with σ_T is the thermal conductivity ($\mathrm{Wm^{-1}\,K^{-1}}$) and ρ is the specific heat ($\mathrm{kg\,m^3}$). All the variables in Eqs. (5) to (9) are defined in Table 1. The relay is assumed to be present in the middle of the $\mathcal{S}$ and $\mathcal{D}$, thereby resulting in identical path loss of the $\mathcal{S} - \mathcal{R}$ and $\mathcal{R} - \mathcal{D}$ links. The path losses are normalized using the path loss of $\mathcal{S} - \mathcal{D}$ link.

3 Performance Analysis

In dual-hop DF relayed UWVLC system, the electrical instantaneous SNR of $\mathcal{S} - \mathcal{R} - \mathcal{D}$ link is

$$\Psi_{SRD} = \min(\Psi_{SR}, \Psi_{RD}^{SC}), \tag{10}$$

where Ψ_{SR} and Ψ_{RD}^{SC} represent the instantaneous values of SNR for $\mathcal{S} - \mathcal{R}$ and $\mathcal{R} - \mathcal{D}$ links, respectively. At the destination node $\mathcal{D}$, the SNR at the output of SC is expressed as

$$\Psi_{RD}^{SC} = \max_{n=1\ldots N} \Psi_{RD}^{(n)}. \tag{11}$$

The instantaneous SNR of the n'th $\mathcal{R} - \mathcal{D}$ link and $\mathcal{S} - \mathcal{R}$ link are represented as $\Psi_{RD}^{(n)}$ and Ψ_{SR}, respectively. They can be computed from Eqs. (1) and (3) as

Table 1 Definition of all variables in Eqs. (5)–(9).

Parameters	Definitions
C_0	0.72
C_1	2.35
χ_T	Dissipation rate of mean square temperature ($K^2\ s^{-3}$)
ϵ	Dissipation rate of turbulent kinetic energy ($m^2\ s^{-3}$)
η	Kolmogorov microscale length
κ	Magnitude of spatial frequency (m^{-1})
P_{TS}	One half of harmonic mean of P_S and P_T
v	Kinematic viscosity ($m^2\ s^{-1}$)
P_S	Prandtl number for salinity
P_T	Prandtl number for temperature
ω	Relative strength of temperature and salinity fluctuation
α	Thermal expansion coefficient l/deg
β	Saline concentration coefficient l/deg
d_r	Eddy diffusivity ratio
Λ	Fresnel ratio of beam at the receiver
Θ	Beam curvature parameter
λ	Wavelength (nm)
k_0	Wave number ($2\pi/\lambda$)

$$\Psi_{SR} = \frac{1}{4} h_{SR}^2 I_{SR}^2 \psi_o \quad \text{and} \quad \Psi_{RD}^{(n)} = \frac{1}{4} h_{RD}^2 I_{RD}^2 \psi_o, \tag{12}$$

where $\psi_o = \eta^2 \mathcal{P}^2 / \sigma_w^2$. The variances of noise are considered to be the same at $\mathcal{R}$ and $\mathcal{D}$ nodes, i.e., $\sigma_{w_D}^2 = \sigma_{w_R}^2 = \sigma_w^2$. Using properties of log-normal random variables, it can be shown that Ψ_{SR} and $\Psi_{RD}^{(n)}$ also follows log-normal distribution. It means

$$\ln(\Psi_{SR}) \sim \mathcal{N}(\mu_{\Psi_{SR}}, \sigma_{\Psi_{SR}}^2), \tag{13}$$

$$\ln(\Psi_{RD}^{(n)}) \sim \mathcal{N}(\mu_{\Psi_{RD}}, \sigma_{\Psi_{RD}}^2), \tag{14}$$

where $\mu_{\Psi_j} = 2\mu_{I_j} + \ln(0.25 h_j^2 \psi_o)$ and $\sigma_{\Psi_j}^2 = 4\sigma_{I_j}^2$.

The cumulative distribution function (CDF) and PDF expressions of end to end, i.e., $\mathcal{S}-\mathcal{R}-\mathcal{D}$, SNR are derived in Ref. 30 as

$$\mathcal{F}_{\Psi_{SRD}}(\psi) = 1 - \mathcal{Q}\left(\frac{\ln(\psi) - \mu_{\Psi_{SR}}}{\sigma_{\Psi_{SR}}}\right) - \mathcal{Q}\left(\frac{\ln(\psi) - \mu_{\Psi_{SR}}}{\sigma_{\Psi_{SR}}}\right) \times \left[1 - \mathcal{Q}\left(\frac{\ln(\psi) - \mu_{\Psi_{RD}}}{\sigma_{\Psi_{RD}}}\right)\right]^N \tag{15}$$

and

$$f_{\Psi_{SRD}}(\psi) = \frac{N}{\sqrt{2\pi}\sigma_{\Psi_{RD}}\Psi} \exp\left(\frac{-(\ln(\psi)-\mu_{\Psi_{RD}})^2}{2\sigma^2_{\Psi_{RD}}}\right)\left[1-\mathcal{Q}\left(\frac{\ln(\psi)-\mu_{\Psi_{RD}}}{\sigma_{\Psi_{RD}}}\right)\right]^{N-1}\mathcal{Q}\left(\frac{\ln(\psi)-\mu_{\Psi_{SR}}}{\sigma_{\Psi_{SR}}}\right) + \frac{1}{\sqrt{2\pi}\sigma_{\Psi_{SR}}\Psi}\exp\left(\frac{-(\ln(\psi)-\mu_{\Psi_{SR}})^2}{2\sigma^2_{\Psi_{SR}}}\right)\left(1+\left[1-\mathcal{Q}\left(\frac{\ln(\psi)-\mu_{\Psi_{RD}}}{\sigma_{\Psi_{RD}}}\right)\right]^N\right), \tag{16}$$

respectively, where $\mathcal{Q}(x) = \frac{1}{\sqrt{2\pi}}\int_x^\infty e^{-t^2/2}\mathrm{d}t$. The CDF expression, when evaluated at the threshold SNR ψ_{th}, results in outage probability of the system.

3.1 *Diversity Gain Analysis*

In this section, we present the analysis for diversity gain by deriving the expressions of RDO and ARDO. For log-normal fading channel, the conventional diversity order does not converge to a specific value. Therefore, our analysis demonstrates the RDO and ARDO by taking a direct $\mathcal{S}-\mathcal{D}$ link as a reference metric. The RDO and ARDO are defined as[31]

$$\mathrm{RDO} = \frac{\partial \ln P^{\mathrm{out}}_{SRD}/\partial \ln \psi_{\mathrm{o}}}{\partial \ln P^{\mathrm{out}}_{SD}/\partial \ln \psi_{\mathrm{o}}}, \tag{17}$$

$$\mathrm{ARDO} = \lim_{\psi_{\mathrm{o}}\to\infty} \mathrm{RDO}, \tag{18}$$

where P^{out}_{SRD} and P^{out}_{SD} are the outage probability of $\mathcal{S}-\mathcal{R}-\mathcal{D}$ and $\mathcal{S}-\mathcal{D}$ link, respectively, defined in Ref. 30 as

$$P^{\mathrm{out}}_{SRD} = \left[1-Q\left(\frac{\ln(\psi_{\mathrm{th}})-2\mu_{I_{SR}}-\ln(h^2_{SR}\psi_{\mathrm{o}}/4)}{2\sigma_{I_{SR}}}\right)\right] + \left[1-Q\left(\frac{\ln(\psi_{\mathrm{th}})-2\mu_{I_{RD}}-\ln(h^2_{RD}\psi_{\mathrm{o}}/4)}{2\sigma_{I_{RD}}}\right)\right]^N - \left[1-Q\left(\frac{\ln(\psi_{\mathrm{th}})-2\mu_{I_{SR}}-\ln(h^2_{SR}\psi_{\mathrm{o}}/4)}{2\sigma_{I_{SR}}}\right)\right]\left[1-Q\left(\frac{\ln(\psi_{\mathrm{th}})-2\mu_{I_{RD}}-\ln(h^2_{RD}\psi_{\mathrm{o}}/4)}{2\sigma_{I_{RD}}}\right)\right]^N, \tag{19}$$

and

$$P^{\mathrm{out}}_{SD} = 1-Q\left(\frac{\ln(\psi_{\mathrm{th}})-2\mu_{I_{SD}}-\ln(\psi_{\mathrm{o}})}{2\sigma_{I_{SD}}}\right). \tag{20}$$

Equation (19) has multiplication of two Q-functions, which is very small and can be ignored. After taking the logarithm of Eqs. (19) and (20), and differentiating with respect to ln (ψ_{o}), and then substituting in Eq. (17), we get the following equation:

$$\mathrm{RDO} = \frac{2\sigma_{I_{RD}}\exp\left(\frac{-1}{2}\left(\frac{\ln(\psi_{\mathrm{o}}/\psi_{th})+2\mu_{I_{SR}}+\ln(h^2_{SR}/4)}{2\sigma_{I_{SR}}}\right)^2\right) + 2N\sigma_{I_{SR}}\left[Q\left(\frac{\ln(\psi_{\mathrm{o}}/\psi_{\mathrm{th}})-2\mu_{I_{RD}}-\ln(h^2_{RD}/4)}{2\sigma_{I_{RD}}}\right)\right]^{N-1}}{Q\left(\frac{\ln(\psi_{\mathrm{o}}/\psi_{\mathrm{th}})+2\mu_{I_{SR}}+\ln(h^2_{SR}/4)}{2\sigma_{I_{SR}}}\right) + \left[Q\left(\frac{\ln(\psi_{\mathrm{o}}/\psi_{\mathrm{th}})-2\mu_{I_{RD}}-\ln(h^2_{RD}/4)}{2\sigma_{I_{RD}}}\right)\right]^N} \frac{2\sigma_{I_{SD}}\exp\left(\frac{-1}{2}\left(\frac{\ln(\psi_{\mathrm{o}}/\psi_{\mathrm{th}})+2\mu_{I_{RD}}+\ln(h^2_{RD}/4)}{2\sigma_{I_{RD}}}\right)^2\right)Q\left(\frac{\ln(\ln(\psi_{\mathrm{o}}/\psi_{\mathrm{th}})+2\mu_{I_{SD}}}{2\sigma_{I_{SD}}}\right)}{\exp\left(\frac{-1}{2}\left(\frac{\ln(\psi_{\mathrm{o}}/\psi_{\mathrm{th}})+2\mu_{I_{SD}}}{2\sigma_{I_{SD}}}\right)^2\right)}. \tag{21}$$

On using the bounds of $Q(\cdot)$ function stated as[32]

$$\frac{\xi\exp(-\xi^2/2)}{(1+\xi^2)\sqrt{2\pi}} < Q(x) < \frac{\exp(-\xi^2/2)}{\xi\sqrt{2\pi}}, \tag{22}$$

and applying the squeezing theorem at high SNR in Eq. (21), we obtain the ARDO as

$$\text{ARDO} = \frac{\sigma^2_{I_{SD}}}{2\sigma_{I_{SR}}\sigma_{I_{RD}}} \times \frac{\frac{2\sigma_{I_{RD}} \exp\left(\frac{-1}{2}\left(\frac{\ln(\psi_o/\psi_{th})+2\mu_{I_{SR}}+\ln\left(\frac{h^2_{SR}}{4}\right)}{2\sigma_{I_{SR}}}\right)^2\right)}{\ln(\psi_\circ)\sqrt{2\pi}} + \frac{2N\sigma_{I_{SR}}(2\sigma_{I_{RD}})^{N-1}\exp\left(\frac{-1}{2}\left(\frac{\ln(\psi_o/\psi_{th})+2\mu_{I_{RD}}+\ln\left(\frac{h^2_{RD}}{4}\right)}{2\sigma_{I_{RD}}}\right)^2\right)^N}{\left(\sqrt{2\pi}\right)^N \ln(\psi_\circ)^N}}{\frac{2\sigma_{I_{SR}} \exp\left(\frac{-1}{2}\left(\frac{\ln(\psi_o/\psi_{th})+2\mu_{I_{SR}}+\ln\left(\frac{h^2_{SR}}{4}\right)}{2\sigma_{I_{SR}}}\right)^2\right)}{\ln(\psi_o)\sqrt{2\pi}} + \frac{(2\sigma_{I_{RD}})^N\exp\left(\frac{-1}{2}\left(\frac{\ln(\psi_o/\psi_{th})+2\mu_{I_{RD}}+\ln\left(\frac{h^2_{RD}}{4}\right)}{2\sigma_{I_{RD}}}\right)^2\right)^N}{\left(\sqrt{2\pi}\right)^N \ln(\psi_o)^N}}. \tag{23}$$

Substituting $e^y = \sum_{k=0}^{n} \frac{y^k}{k!}$ into Eq. (23) and neglecting the higher order terms, we get

$$\text{ARDO} = \frac{(\sigma_{I_{SD}})^2}{\sigma_{I_{SR}}\sigma_{I_{RD}}} \times \frac{(2\sigma_{I_{RD}})^3\left(\sqrt{2\pi}\right)^N \ln(\psi_o)^{N-2} + N^2(2\sigma_{I_{SR}})^3(2\sigma_{I_{RD}})^{N-1}\left(\sqrt{2\pi}\right)\ln(\psi_o)^{-1}}{(2\sigma_{I_{RD}})^2(2\sigma_{I_{SR}})\left(\sqrt{2\pi}\right)^N \ln(\psi_o)^{N-2} + N(2\sigma_{I_{SR}})^2(2\sigma_{I_{RD}})^N\left(\sqrt{2\pi}\right)\ln(\psi_o)^{-1}}. \tag{24}$$

Evaluating Eq. (24) at $\psi_o \to \infty$, we obtain the simplified expression of ARDO as

$$\text{ARDO} \approx \frac{\sigma^2_{I_{SD}}}{\sigma^2_{I_{SR}}}. \tag{25}$$

Note that ARDO is the ratio of scintillation index of $\mathcal{S}-\mathcal{D}$ to $\mathcal{S}-\mathcal{R}$ links and does not depend on N, and scintillation index $\mathcal{R}-\mathcal{D}$ link. This happens because the instantaneous SNR of $\mathcal{S}-\mathcal{R}-\mathcal{D}$ link is computed as the SNR of the weakest link in Eq. (10), and in the considered system $\mathcal{S}-\mathcal{R}$ is the weakest link due to diversity applied in the $\mathcal{R}-\mathcal{D}$ link.

3.2 *ASEP Analysis*

In this section, we derive the analytical expressions of ASEP for M-ary PAM and M-ary SQAM. The conditional symbol error probability with these modulation schemes in the presence of AWGN is given as[33]

$$P_s(e|\Psi) = A\mathcal{Q}\left(\sqrt{C\Psi}\right), \tag{26}$$

where $A = 2(M-1)/(M\log_2 M)$ and $C = 3/((M-1)(2M-1))$ for M-ary PAM, and $A = 2(\sqrt{M}-1)/\sqrt{M}$ and $C = 3/(M-1)$ for M-ary QAM with M is the constellation size.

The ASEP of the UWVLC system is computed using PDF-based approach. The expression for ASEP can be expressed as

$$\overline{P}_s = E[P_s(e|\Psi_{SRD})] = E\left[A\mathcal{Q}\left(\sqrt{C\Psi_{SRD}}\right)\right] = \int_0^\infty A\mathcal{Q}\left(\sqrt{C\psi}\right) f_{\Psi_{SRD}}(\psi)\mathrm{d}\psi, \tag{27}$$

where $E[\cdot]$ is the expectation operator, $P_s(e|\Psi)$ is the conditional SEP for AWGN channel, and $f_{\Psi_{SRD}}(\psi)$ is the PDF of the instantaneous SNR of the received signal at receiver.

Let us assume $\mathcal{K}(\Psi_{SRD})$ is an arbitrary function of Ψ_{SRD} whose PDF is given in Eq. (16). Then

$$E[\mathcal{K}(\Psi_{SRD})] = \int_0^\infty \mathcal{K}(\psi) f_{\Psi_{SRD}}(\psi)\mathrm{d}\psi. \tag{28}$$

On substituting the PDF of Ψ_{SRD} from Eq. (16) into Eq. (28), we get

$$\begin{aligned}E[\mathcal{K}(\Psi_{SRD})] = &\frac{N}{\sqrt{2\pi}\sigma_{\Psi_{RD}}}\int_0^\infty \mathcal{K}(\psi)\psi\ \exp\left(\frac{-(\ln(\psi)-\mu_{\Psi_{RD}})^2}{2\sigma^2_{\Psi_{RD}}}\right)\\ &\times\left(1+\left[1-\mathcal{Q}\left(\frac{\ln(\psi)-\mu_{\Psi_{RD}}}{\sigma_{\Psi_{RD}}}\right)\right]^{N-1}\right)\\ &\times\mathcal{Q}\left(\frac{\ln(\psi)-\mu_{\Psi_{SR}}}{\sigma_{\Psi_{SR}}}\right)\mathrm{d}\psi+\frac{1}{\sqrt{2\pi}\sigma_{\Psi_{SR}}}\int_0^\infty\frac{\mathcal{K}(\psi)}{\psi}\ \exp\left(\frac{-(\ln(\psi)-\mu_{\Psi_{SR}})^2}{2\sigma^2_{\Psi_{SR}}}\right)\\ &\times\left(1+\left[1-\mathcal{Q}\left(\frac{\ln(\psi)-\mu_{\Psi_{RD}}}{\sigma_{\Psi_{RD}}}\right)\right]^{N}\right)\mathrm{d}\psi.\end{aligned} \tag{29}$$

On performing the change of variables, $x_1=\frac{(\ln(\psi)-\mu_{\Psi_{RD}})}{\sqrt{2}\sigma_{\Psi_{RD}}}$ and $x_2=\frac{(\ln(\psi)-\mu_{\Psi_{SR}})}{\sqrt{2}\sigma_{\Psi_{SR}}}$ in the first and second integral, respectively, of Eq. (29) and after simplifying, we get

$$\begin{aligned}E[\mathcal{K}(\Psi_{SRD})] = N&\int_{-\infty}^\infty \mathcal{K}\left(\sqrt{C\ \exp\left(\sqrt{2}\sigma_{\Psi_{RD}}x_1+\mu_{\Psi_{RD}}\right)}\right)\exp\left(x_1\sqrt{2}\sigma_{\Psi_{RD}}\right)^2\\ &\times\left(1+\left[1-\mathcal{Q}\left(\frac{\exp\left(\sqrt{2}\sigma_{\Psi_{RD}}x_1+\mu_{\Psi_{RD}}\right)-\mu_{\Psi_{RD}}}{\sigma_{\Psi_{RD}}}\right)\right]^{N-1}\right)\\ &\times\mathcal{Q}\left(\frac{\exp\left(\sqrt{2}\sigma_{\Psi_{SR}}x_2+\mu_{\Psi_{SR}}\right)-\mu_{\Psi_{SR}}}{\sigma_{\Psi_{SR}}}\right)e^{-x_1^2}\mathrm{d}x_1\\ &+\int_{-\infty}^\infty \mathcal{K}\left(\sqrt{C\ \exp\left(\sqrt{2}\sigma_{\Psi_{SR}}x_2+\mu_{\Psi_{SR}}\right)}\right)\exp\left(x_2\sqrt{2}\sigma_{\Psi_{SR}}\right)^2\\ &\times\left(1+\left[1-\mathcal{Q}\left(\frac{\exp\left(\sqrt{2}\sigma_{\Psi_{RD}}x_1-\mu_{\Psi_{RD}}\right)}{\sigma_{\Psi_{RD}}}\right)\right]^{N}\right)e^{-x_2^2}\mathrm{d}x_2.\end{aligned} \tag{30}$$

Using Gauss Hermite quadrature technique $\int_{-\infty}^\infty \exp(x^2)f(x)\mathrm{d}x\approx\sum_{i=1}^n w_i f(x_i)$[34] in Eq. (30), we obtain Eq. (31) as

$$\begin{aligned}E[\mathcal{K}(\Psi_{SRD})] = &\frac{N}{\sqrt{\pi}}\sum_{i=1}^n w_i\left(\mathcal{K}\sqrt{C\exp\left(\sqrt{2}\sigma_{\Psi_{RD}}x_{1i}+\mu_{\Psi_{RD}}\right)}\right)\\ &\times\left(1+\left[1-\mathcal{Q}\left(\frac{\sqrt{2}\sigma_{\Psi_{RD}}x_{1i}+\mu_{\Psi_{RD}}-\mu_{\Psi_{RD}}}{\sigma_{\Psi_{RD}}}\right)\right]^{N-1}\right)\\ &\times\mathcal{Q}\left(\frac{\sqrt{2}\sigma_{\Psi_{RD}}x_{1i}+\mu_{\Psi_{RD}}-\mu_{\Psi_{SR}}}{\sigma_{\Psi_{SR}}}\right)+\frac{1}{\sqrt{\pi}}\sum_{i=1}^n w_i\left(\mathcal{K}\sqrt{C\exp\left(\sqrt{2}\sigma_{\Psi_{SR}}x_{2i}+\mu_{\Psi_{SR}}\right)}\right)\\ &\times\left(1+\left[1-\mathcal{Q}\left(\frac{\sqrt{2}\sigma_{\Psi_{SR}}x_{1i}+\mu_{\Psi_{SR}}-\mu_{\Psi_{RD}}}{\sigma_{\Psi_{RD}}}\right)\right]^{N}\right).\end{aligned} \tag{31}$$

Now taking $\mathcal{K}(\Psi_{SRD})=A\mathcal{Q}(\sqrt{C\Psi_{SRD}})$ and substituting in Eq. (31), the ASEP equation can be expressed as

$$\overline{P_s} = \frac{N}{\sqrt{\pi}}\sum_{i=1}^{n} w_i\left(\mathcal{Q}\sqrt{C\exp\left(\sqrt{2}\sigma_{\Psi_{RD}}x_{1i}+\mu_{\Psi_{RD}}\right)}\right) \times\left(1+\left[1-\mathcal{Q}\left(\frac{\sqrt{2}\sigma_{\Psi_{RD}}x_{1i}+\mu_{\Psi_{RD}}-\mu_{\Psi_{RD}}}{\sigma_{\Psi_{RD}}}\right)\right]^{N-1}\right) \times\mathcal{Q}\left(\frac{\sqrt{2}\sigma_{\Psi_{RD}}x_{1i}+\mu_{\Psi_{RD}}-\mu_{\Psi_{SR}}}{\sigma_{\Psi_{SR}}}\right)+\frac{1}{\sqrt{\pi}}\sum_{i=1}^{n} w_i\left(A\mathcal{Q}\sqrt{C\exp\left(\sqrt{2}\sigma_{\Psi_{SR}}x_{2i}+\mu_{\Psi_{SR}}\right)}\right) \times\left(1+\left[1-\mathcal{Q}\left(\frac{\sqrt{2}\sigma_{\Psi_{SR}}x_{2i}+\mu_{\Psi_{SR}}-\mu_{\Psi_{RD}}}{\sigma_{\Psi_{RD}}}\right)\right]^{N}\right), \tag{32}$$

where w_i and x_{li}, $l \in \{1,2\}$ are the weight factors and zeros of n'th order Gauss Hermite polynomial, respectively.

3.3 *Ergodic Capacity*

The instantaneous channel capacity of a dual-hop cooperative OWC system can be calculated as[35]

$$C_e(\Psi_{SRD}) \approx \frac{1}{2}\log_2\left(1+\frac{\exp(1)}{2\pi}\Psi_{SRD}\right)\ \text{bits/s}. \tag{33}$$

We derive the ergodic capacity of the UWVLC dual-hop system by taking the expectation of Eq. (33):

$$\overline{C_e} \approx E[C_e(\Psi_{SRD})] = \int_0^\infty C_e(\psi)f_{\Psi_{SRD}}(\psi)\mathrm{d}\psi. \tag{34}$$

$$\overline{C_e} = \frac{1}{2}\int_0^\infty \log_2\left(1+\frac{\exp(1)}{2\pi}\psi\right)f_{\Psi_{SRD}}(\psi)\mathrm{d}\psi. \tag{35}$$

Now, taking $\mathcal{K}(\Psi_{SRD}) = \log_2(1+\frac{\exp(1)}{2\pi}\Psi_{SRD})$ and using Eq. (31), we get the closed form expression of ergodic capacity as

$$\overline{C_e} \approx 0.56\sum_{i=1}^{n} w_i(\log_2(1+\exp(1.414\sigma_{\Psi_{SR}}x_{2i}+\mu_{\Psi_{SR}}))^{0.5}) \times\left(1+\left[1-\mathcal{Q}\left(\frac{1.414\sigma_{\Psi_{SR}}x_{2i}+\mu_{\Psi_{SR}}-\mu_{\Psi_{RD}}}{\sigma_{\Psi_{RD}}}\right)\right]^{N}\right) +0.56N\sum_{i=1}^{n} w_i(\log_2[1+\exp(1.414\sigma_{\Psi_{RD}}x_{1i}+\mu_{\Psi_{RD}})^{0.5}]) \times\left(1+\left[1-\mathcal{Q}\left(\frac{1.414\sigma_{\Psi_{RD}}x_{1i}+\mu_{\Psi_{RD}}-\mu_{\Psi_{RD}}}{\sigma_{\Psi_{RD}}}\right)\right]^{N-1}\right) \times\mathcal{Q}\left(\frac{1.414\sigma_{\Psi_{RD}}x_{1i}+\mu_{\Psi_{RD}}-\mu_{\Psi_{SR}}}{\sigma_{\Psi_{SR}}}\right). \tag{36}$$

4 Numerical and Simulation Results

In this section, we present analytical results of the proposed dual-hop UWVLC system in terms of outage probability, ASEP, and channel capacity versus average SNR ψ_o. The system performance is presented for different values of turbulence, taking two values of temperature 20°C and 30°C. The distance L between source and destination is 20 m, and the relay is placed in the middle. The salinity is considered to be 35 PPT (parts per thousand) in both cases of temperature.

Table 2 Temperature-dependent parameters of spatial power spectrum.

Parameters		Temperature = 20°C	Temperature = 30°C
Kinematic viscosity	v	1.05×10^{-6} m^2 s^{-1}	8.42×10^{-7} m^2 s^{-1}
Prandtl number for salinity	P_S	715.60	559.71
Prandtl number for temperature	P_T	7.16	5.60
Thermal expansion coefficient	α	2.57×10^{-4} l/deg	3.33×10^{-4} l/deg
Saline concentration coefficient	β	7.32×10^{-4} l/deg	7.16×10^{-4} l/deg

We assume coastal water has an extinction coefficient $c = 0.305$ and correction coefficient $\mathcal{T} = 0.13$. The parameters such as $(P_T, P_S, \alpha, \beta, v)$ of the spatial power spectrum model $\phi_n(\kappa)$ depend on the temperature and salinity of water.[9,10,18] Yao et al.[36] provided numerical expressions for calculating the parameters mentioned above for a wide range of average temperature and salinity concentration. Further, Ata et al.[37] analyzed the BER for any temperature and salinity concentration. We have considered the values of the temperature-dependent parameters as defined in Ref. 22, which are calculated using TEOS-10 and FVCOM MATLAB toolboxes.

Based on the calculated values mentioned in Ref. 22, Tables 2 and 3 in conjunction with Eqs. (7)–(9), the scintillation index is calculated. The scintillation indices for two different temperatures 20°C and 30°C at link distance 20 m are 2.55×10^{-1} and 4.13×10^{-1}, respectively, and at distance 10 m, are $\sigma_I^2 = 0.32 \times 10^{-1}$ and $\sigma_I^2 = 0.57 \times 10^{-1}$, respectively. Based on the scintillation indices of two temperatures, the parameters of power spectrum model, given in Table 1,[22] we generate a log-normal channel, as shown in the system model and present simulation results.

We perform the Monte Carlo simulation using MATLAB. We generate $N_{\text{sym}} = 10^6$ IID M-PAM/RQAM symbols with average energy normalized to 1. The direct current (DC) bias is added to the generated symbols to move these symbols to the first quadrant. For every iteration, we generate path loss using Eq. (4) and N samples of lognormally distributed irradiance using Eq. (2). The received signal model given in Eq. (1) is computed considering $\eta_\circ = 1$, $P = 1$. We assume perfect CSI at R. The DC bias is removed, and the received symbols are equalized using zero-forcing equalizer following symbol detection. The similar steps are implemented to simulate the signal received at D via $N - \mathcal{R} - \mathcal{D}$ links as given by Eq. (3). The $\mathcal{S} - \mathcal{R} - \mathcal{D}$ instantaneous SNRs of N links are evaluated using Eq. (10), and the link with maximum SNR is identified. The received signal over the identified maximum SNR link is equalized and used for detection. The simulation results are closely matching with their analytical counterparts.

In Fig. 2, we present the outage probability versus average SNR $\psi_\circ$ for the different numbers of photodetectors N at a temperature of 20°C. The direct link without relay is also included for comparing the system performance with receiver diversity. It is observed that the derived

Table 3 Path loss and turbulence parameter values.

Parameters	Values
Q_F	6 deg
D_R	5 cm
η	0.5 W/A
ϵ	1×10^{-2}
ω	−3
χ_T	1×10^{-5} K^2 S^{-3}
λ	530 nm

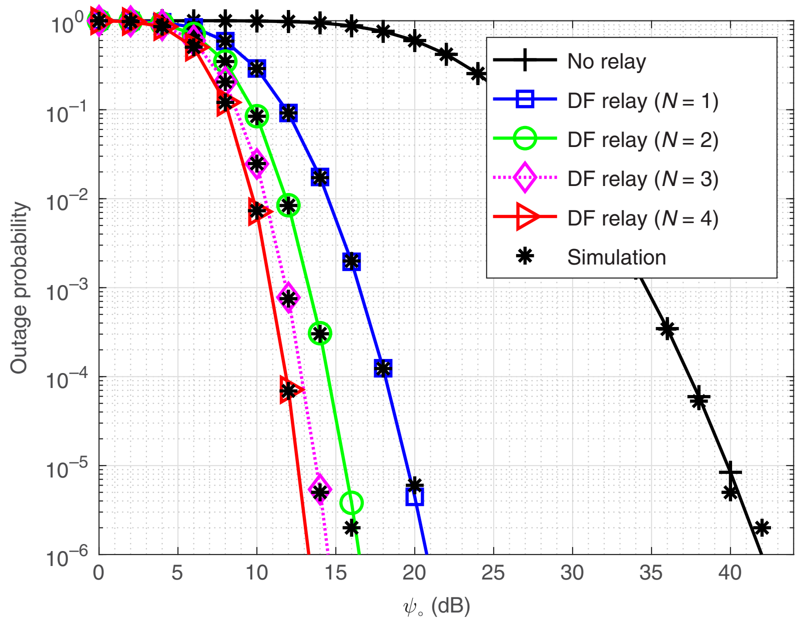

Fig. 2 Outage probability for different numbers of receivers at temperature of 20°C.

analytical expressions are closely matching with the simulated results. For the targeted outage probability of 10^{-5}, SNR of 39.8 dB is required in the direct link without relay, whereas for the same outage probability, the SNR reduces to 19.4, 15.6, 13.9, and 12.5 dB for $N = 1$, 2, 3, and 4, respectively.

In Fig. 3, we present the outage probability versus average SNR ψ_{o} for the different numbers of photodetectors N at a temperature of 30°C. For the outage probability of 10^{-5}, the required SNRs are 23.4, 18.1, 15.9, and 14.1 dB for $N = 1$,2, 3, and 4, respectively. From Figs. 1 and 2, it can be seen that the increase in temperature of seawater severely degrades system performance. In other words, the strength of turbulence increases with temperature and its adverse effect is visible on the performance.

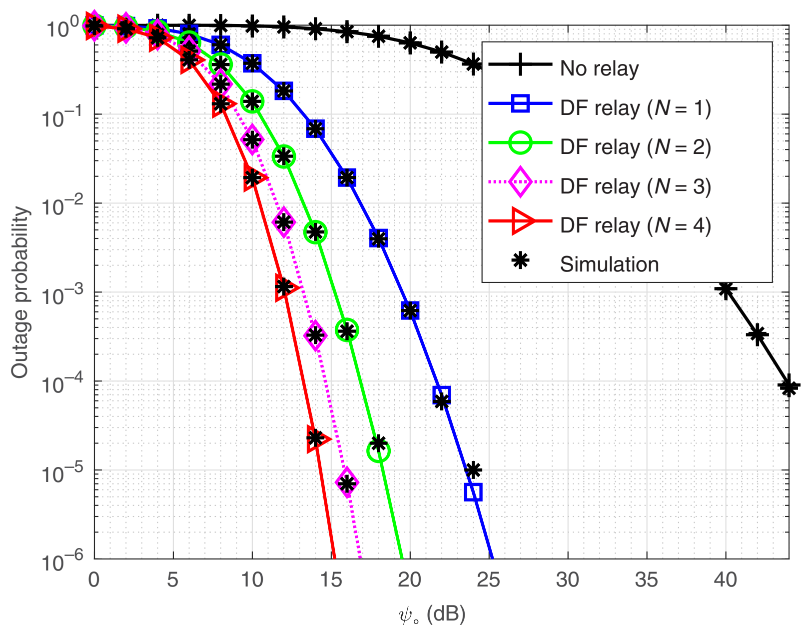

Fig. 3 Outage probability for different numbers of receivers at temperature of 30°C.

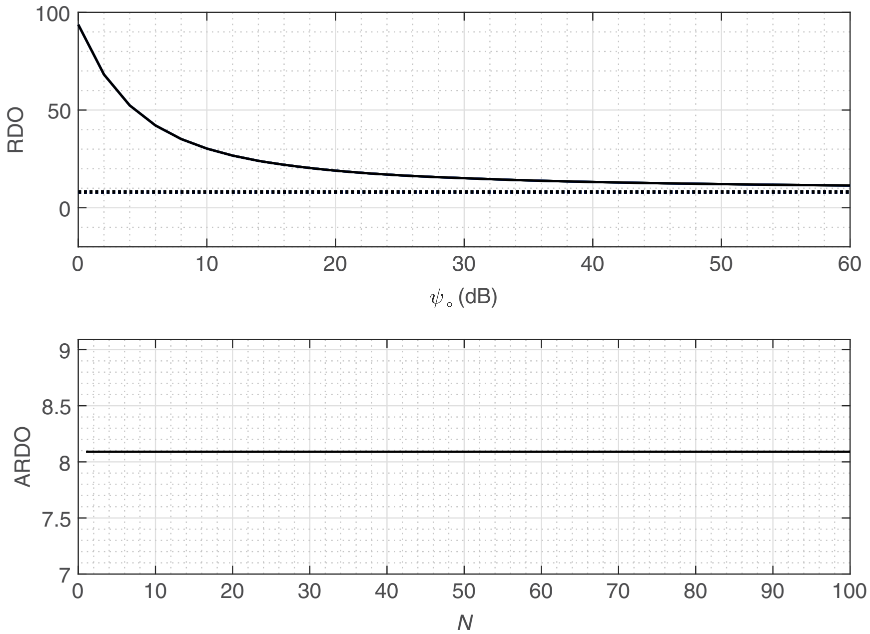

Fig. 4 RDO for different numbers of receivers.

In Fig. 4, we illustrate the RDO versus average SNR ψ_o, and ARDO versus N photodetctors for the considered system. From Eq. (18) and using the values of scintillation index stated above, the theoretical ARDO is calculated as 8.02. It is observed that the RDO converges to ARDO at a high-average SNR, thereby confirming the analytical results. Further, the acheived diversity gain of 8.02 is due to employing cooperative relay when compared to non-cooperative direct link. However, the number of photodetectors at the destination has no effect on the diversity order. This is an important observation as it suggests that in dual-hop cooperative communication using spatial diversity in either $\mathcal{S}-\mathcal{R}$ or $\mathcal{R}-\mathcal{D}$ link (but not both) does not provide any further diversity gain. Nevertheless, an increase in temperature also does not change the diversity order.

In Fig. 5, we present the ASEP versus average SNR ψ_o for four-PAM and four-SQAM modulation schemes. We also consider without relay and with relay for different photodetectors N.

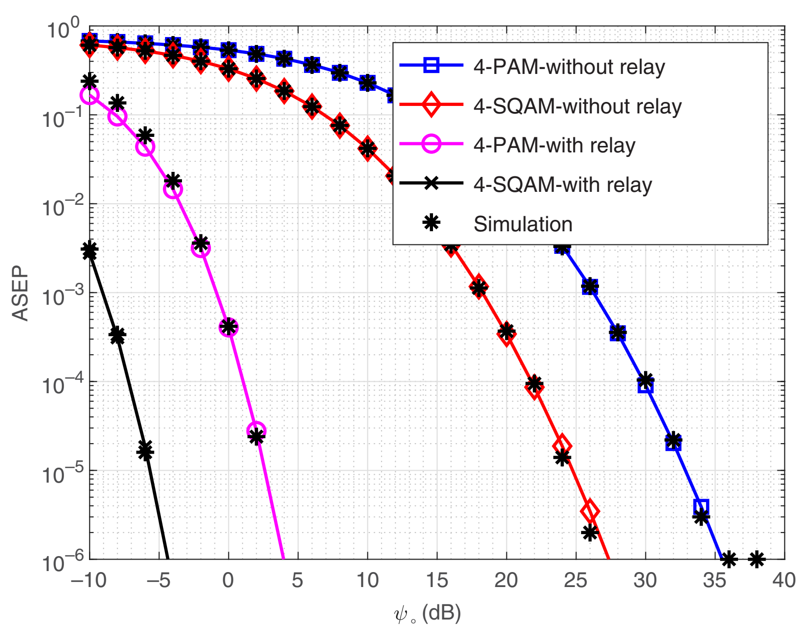

Fig. 5 ASEP for four-PAM and four-SQAM modulation schemes with relay and without relay.

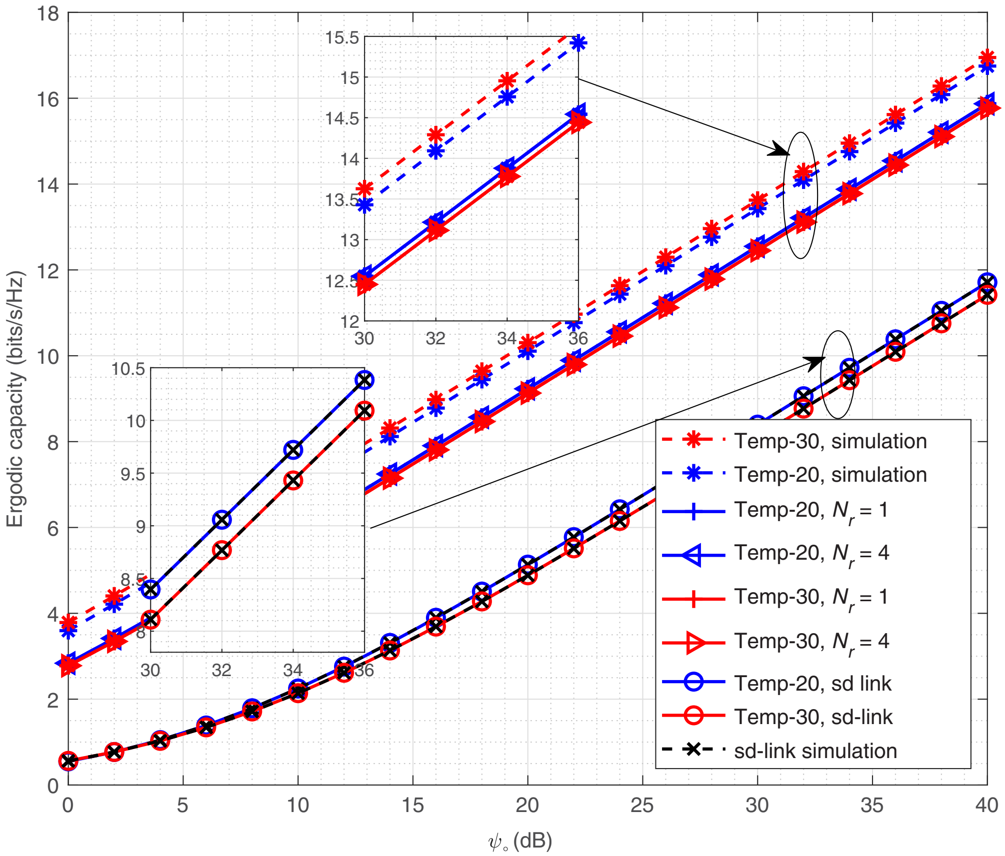

Fig. 6 Ergodic capacity at 20°C and 30°C temperature.

A close matching between analytical and simulation results is observed. In order to achieve a targeted ASEP of 10^{-4}, SNR = 30 dB is required considering four-PAM scheme for SISO ($N = 1$) link. However, it decreases to 1 dB for the relay assisted system for $N = 2$. Furthermore, with four-SQAM, 24.5 dB less SNR is required with relay for the same ASEP and N, which indicates significant performance improvement with the four-SQAM modulation scheme.

In Fig. 6, we compare the analytical and simulation results of ergodic capacity versus average SNR for both relayed and non-relayed cases considering temperature as (20°C, 30°C), and N as (1, 4). Our results demonstrate the adverse effect of an increase in temperature on the system capacity. For example, to achieve the capacity of 10 bps/Hz, an average SNRs of 34.7 and 36 dB are required for 20°C and 30°C temperatures, respectively; whereas in relayed system, an average SNRs of 22 and 22.8 dB are required for 20°C and 30°C temperatures, respectively. Further, it is observed that increasing the number of photodetectors at D does not have any effect on the ergodic capacity, for both relayed and non-relayed cases.

5 Conclusion

We presented a dual-hop cooperative UWVLC system with N photodetectors at the destination. We considered DF relay at the middle of source and destination. We modeled the underlying channel with path loss and log-normal distribution, where the statistical parameters of log-normal distribution depend on turbulence, which varies with the temperature of sea water. We selected one out of N photodetectors for detection based on received SNR and derived the analytical expression of ASEP for four PAM and four SQAM schemes using Gauss Hermite quadrature integral method. We conducted diversity analysis and also derived closed-form expression of ergodic channel capacity for the considered system. We also presented simulation results for the same and observed close matching between simulations and analytical results.

We conclude that the increase in temperature of seawater degrades the performance of the system. However, by increasing the number of photodetectors N, the degradation in the performance can be reduced. Furthermore, we presented the ASEP results with relay and without relay for PAM and SQAM modulation schemes. Above all, we studied the ergodic capacity of the system for different scenarios draw useful insights.

References

1. Z. Zeng et al., "A survey of underwater optical wireless communications," *IEEE Commun. Surveys Tuts.* **19**, 204–238 (2016).
2. C. M. Gussen et al., "A survey of underwater wireless communication technologies," *J. Commun. Inf. Sys.* **31**, 242–255 (2016).
3. H. Kaushal and G. Kaddoum, "Underwater optical wireless communication," *IEEE Access* **4**, 1518–1547 (2016).
4. A. Yilmaz, M. Elamassie, and M. Uysal, "Diversity gain analysis of underwater vertical MIMO VLC links in the presence of turbulence," in *IEEE Int. Black Sea Conf. Commun. and Networking (BlackSeaCom)*, pp. 1–6 (2019).
5. C. Shen et al., "Going beyond 10-meter, gbit/s underwater optical wireless communication links based on visible lasers," in *Proc. 2017 Opto-Electron. Commun. Conf. Photon. Global Conf.*, pp. 1–3 (2017).
6. N. Anous et al., "Performance evaluation of LOS and NLOS vertical inhomogeneous links in underwater visible light communications," *IEEE Access* **6**, 22408–22420 (2018).
7. S. Corporation, "Bluecomm underwater optical communication," 2020, https://www.sonardyne.com/product/bluecomm-underwater-optical-communication-system/.
8. R. Chester and T. D. Jickells, *Marine Geochemistry*, 3rd ed., Wiley Black Well (2012).
9. O. Korotkova, "Light propagation in a turbulent ocean," *Prog. Opt.* **64**, 1–43 (2019).
10. R. Millard and G. Seaver, "An index of refraction algorithm for seawater over temperature, pressure, salinity, density and wavelength," *Deep Sea Res. Part A. Oceanogr. Res. Pap.* **37**, 1909–1926 (1990).
11. M. Elamassie, F. Miramirkhani, and M. Uysal, "Performance characterization of underwater visible light communication," *IEEE Trans. Commun.* **67**, 543–552 (2019).
12. F. Akhoundi, J. A. Salehi, and A. Tashakori, "Cellular underwater wireless optical CDMA network: performance analysis and implementation concepts," *IEEE Trans. Commun.* **63**, 882–891 (2015).
13. C. Wang, H.-Y. Yu, and Y.-J. Zhu, "A long distance underwater visible light communication system with single photon avalanche diode," *IEEE Photonics J.* **8**, 1–11 (2016).
14. M. Elamassie et al., "Effect of eddy diffusivity ratio on underwater optical scintillation index," *J. Opt. Soc. Am. A* **34**, 1969–1973 (2017).
15. M. Elamassie and M. Uysal, "Performance characterization of vertical underwater VLC links in the presence of turbulence," in *11th Int. Symp. Commun. Syst., Networks Digital Signal Process. (CSNDSP)*, pp. 1–6 (2018).
16. S. Ghasvarianjahromi et al., "Simultaneous lightwave information and power transfer in underwater visible light communications," in *IEEE 30th Annu. Int. Symp. Person., Indoor and Mob. Radio Commun. (PIMRC)*, pp. 1–6 (2019).
17. M. Elamassie, S. M. Sait, and M. Uysal, "Underwater visible light communications in cascaded gamma–gamma turbulence," in *IEEE Globecom Workshops (GC Wkshps)*, pp. 1–6 (2018).
18. M. Elamassie and M. Uysal, "Vertical underwater visible light communication links: channel modeling and performance analysis," *IEEE Trans. Wireless Commun.* **19**(10), 6948–6959 (2020).
19. Z. Vali et al., "Experimental study of the turbulence effect on underwater optical wireless communications," *Appl. Opt.* **57**, 8314–8319 (2018).
20. K. P. Peppas, A. C. Boucouvalas, and Z. Ghassemloy, "Performance of underwater optical wireless communication with multi-pulse pulse-position modulation receivers and spatial diversity," *IET Opt.* **11**, 180–185 (2017).

21. M. V. Jamali, P. Nabavi, and J. A. Salehi, "MIMO underwater visible light communications: comprehensive channel study, performance analysis, and multiple-symbol detection," *IEEE Trans. Veh. Technol.* **67**, 8223–8237 (2018).
22. M. Elamassie et al., "Transmit laser selection for underwater visible light communication systems," in *IEEE 30th Annu. Int. Symp. Person. Indoor and Mob. Radio Commun. (PIMRC)*, pp. 1–6 (2019).
23. M. Elamassie and M. Uysal, "Asymptotic performance of generalized transmit laser selection over lognormal turbulence channels," *IEEE Commun. Lett.* **24**(8), 1762–1766 (2020).
24. P. Zou et al., "Enhanced performance of odd order square geometrical shaping QAM constellation in underwater and free space VLC system," *Opt. Commun.* **438**, 132–140 (2019).
25. M. Cheng et al., "Channel capacity of the OAM-based free-space optical communication links with Bessel–Gauss beams in turbulent ocean," *IEEE Photonics J.* **8**, 1–11 (2016).
26. E. J. Lee and V. W. S. Chan, "Part 1: optical communication over the clear turbulent atmospheric channel using diversity," *IEEE J. Sel. Areas Commun.* **22**(9), 1896–1906 (2004).
27. S. Jaruwatanadilok, "Underwater wireless optical communication channel modeling and performance evaluation using vector radiative transfer theory," *IEEE J. Sel. Areas Commun.* **26**, 1620–1627 (2008).
28. E. J. Shin and V. W. S. Chan, "Optical communication over the turbulent atmospheric channel using spatial diversity," in *Global Telecommun. Conf., 2002. GLOBECOM '02*, IEEE, Vol. 3, pp. 2055–2060 (2002).
29. M. Cheng, L. Guo, and Y. Zhang, "Scintillation and aperture averaging for Gaussian beams through non-kolmogorov maritime atmospheric turbulence channels," *Opt. Exp.* **23**(25), 32606–32621 (2015).
30. K. K. Garg and V. Bhatia, "Performance analysis of cooperative NLOS UVC system with receiver diversity," in *Natl. Conf. Commun. (NCC)*, IEEE, pp. 1–6 (2020).
31. M. Safari and M. Uysal, "Cooperative diversity over log-normal fading channels: performance analysis and optimization," *IEEE Trans. Wireless Commun.* **7**, 1963–1972 (2008).
32. J. G. Proakis and M. Salehi, *Digital Communications*, 5th ed., McGraw-Hill (2008).
33. A. Goldsmith, *Wireless Communications*, Cambridge University Press (2005).
34. M. Abramowitz and I. A. Stegun, *Handbook of Mathematical Functions (National Bureau of Standards, Washington, DC, 1972)*, 10th ed., Dover Publications (1972).
35. L. Yin and H. Haas, "Physical-layer security in multiuser visible light communication networks," *IEEE J. Sel. Area Commun.* **36**(1), 162–174 (2017).
36. J.-R. Yao, M. Elamassie, and O. Korotkova, "Spatial power spectrum of natural water turbulence with any average temperature, salinity concentration, and light wavelength," *J. Opt. Soc. Am. A* **37**, 1614–1621 (2020).
37. Y. Ata, J. Yao, and O. Korotkova, "BER variation of an optical wireless communication system in underwater turbulent medium with any temperature and salinity concentration," *Opt. Commun.* **485**, 126751 (2021).

Rachna Sharma has received her MTech degree in communication systems and signal processing from Jaypee Institute of Information Technology, Noida, India, in 2007. She is working as an assistant professor in the Electronics and Communication Department at the School of Technology, Nirma University, Ahmedabad, India. Currently, she is pursuing her PhD in wireless communications at Nirma University. Her area of interest includes wireless communication, underwater communication.

Yogesh N. Trivedi received his PhD in electrical engineering from the Indian Institute of Technology, Kanpur, India, in 2011. Currently, he is a professor with the Department of Electronics and Communication Engineering, School of Technology, Nirma University, Ahmedabad, India. He has authored or co-authored several papers in national/international conferences and international journals. His current research interests include signal processing, wireless communications, and cognitive radio.